Scintillating and decorrelating signals for different propagation paths in a random medium

(article starts on next page)

Scintillating and decorrelating signals for different propagation paths in a random medium

Jens Forssén

Division of Applied Acoustics, Department of Architecture and Civil Engineering, Chalmers University of Technology, SE-412 96 Gothenburg, Sweden

ARTICLE INFO

ABSTRACT

Randomness in the medium of propagation affects the signal received at a distance from a source resulting in amplitude and phase fluctuations as well as reduced coherence between different paths of propagation. A method is described and validated for incorporating such fluctuations and decorrelations in sound signals in a single approach. Here, simplified conditions are used of open space, with or without a single reflecting surface, assuming fluctuations as for plane waves in homogeneous and isotropic temperature turbulence. Validating results are shown for Gaussian and von Karman turbulence models and exemplifying sound clips are provided as supplementary material.

1. Introduction

Randomness in acoustic propagation conditions affects the signal at a receiver placed at a distance from the source. Without any reflecting surface the randomnesses of the propagation medium cause fluctuations in amplitude and phase of the received signal, i.e. random amplitude fluctuations (scintillations) and random time delays, which can be seen as a distortion of the received signal compared with a free-field signal that has not been subjected to a random medium. In the presence of wave reflecting surfaces, enabling additional paths of propagation, other distorted versions of the free-field signal are added to the received signal. This will affect the correlation between the direct signal and the reflected signal, usually described by a mutual coherence function that may depend on the transverse separation distance between the two paths, range of propagation, sound frequency and the strength of the medium randomnesses, e.g. in terms of spectra of temperature and velocity fluctuations due to atmospheric turbulence (see e.g. [1]).

Models for the coherence between the direct signal and a reflected signal have been derived for a large variety of cases using frequency domain approaches. However, for time-domain signals, modelling tools need further development, e.g. for the purpose of auralizing environmental noise sources in motion, like road vehicles, trains, aeroplanes, drones, and wind turbine rotor blades. Such an application is of interest in the current paper, where the effect of a random medium is modelled for direct and reflected sound from a non-stationary source to a stationary receiver.

In the recent decade, development in the area of auralization of randomly fluctuating environmental sounds, caused by randomness in the propagation conditions, to a large part targets the effects of atmospheric randomnesses on amplitude and phase fluctuations for a single path of propagation (e.g. [2–4]). For modelling the effect of mutual coherence between multiple receiver pairs, the effect of the ground reflection on the expected value of the total amplitude has been treated [5]. Also, an approach using multiple uncorrelated source signals as input has been developed (see [6], based on [7]). The approach is however not applicable to the current work, where the noise sources of interest may emit characteristic signals, e.g. an internal combustion engine sound with a combination of tones, noise and repeated impulses, i.e. where the sounds from the different paths of propagation are not suitable to be modelled as independent noise signals. Furthermore, the effect of reduced coherence between direct and ground reflected propagation paths has been modelled using a time-domain filtering technique allowing for a frequency dependent partial decorrelation; however, under the assumption of independent frequency components and where the random fluctuations of the sound were modelled in a separate process [8].

The current paper presents a method that includes the random fluctuations of the received signals and the decorrelation effect in a single approach, as presented and exemplified below. In Section 2, the theoretical framework and the modelling approach are described. First, the relevant parts of the theory for sound propagation in a turbulent atmosphere are summarised, largely based on works by Ostashev et al. (e.g. [1]). Thereafter, the section is concluded with a description of how the

presented theory can be used to create realisations of sound signals fulfilling the wanted characteristics of fluctuations and decorrelation.

In Section 3, application examples are presented. First, it is demonstrated how time signals can be created that produce the desired coherence as a function of both frequency and space. Thereafter, the method is demonstrated for a situation with a moving source and a reflecting surface. Section 4 concludes the paper, followed by suggestions for further work.

2. Method

2.1. Theoretical framework for the effects of a turbulent atmosphere

For the complex-valued sound pressure amplitude, p, at two points in space, $\mathbf{r_1}$ and $\mathbf{r_2}$, at the same propagation range, x, from the source (see Fig. 2), the *transverse mutual coherence function*, Γ, can be defined as [1, Eq. 7.154]

$$\Gamma(x; \mathbf{r_1}, \mathbf{r_2}) = \langle p(x, \mathbf{r_1}) p^*(x, \mathbf{r_2}) \rangle \tag{1}$$

where $\langle \rangle$ denotes expected value. In terms of the *complex phase*, $\Psi = \chi + \mathrm{i}\phi$, which describes the random fluctuations, the pressure amplitude can be written as

$$p(x, \mathbf{r}) = \hat{p}(x, \mathbf{r}) \mathrm{e}^{\chi(x, \mathbf{r}) + \mathrm{i}\phi(x, \mathbf{r})} \tag{2}$$

where $\hat{p}$ is the amplitude in absence of the randomness of the medium. For the *log-amplitude*, χ, and the *phase*, ϕ, the corresponding transverse correlation functions can be defined as

$$B_\chi = \langle \chi(x, \mathbf{r_1}) \chi(x, \mathbf{r_2}) \rangle \tag{3}$$

$$B_\phi = \langle \phi(x, \mathbf{r_1}) \phi(x, \mathbf{r_2}) \rangle. \tag{4}$$

The mutual coherence function, Γ, can be written as function of the log-amplitude and phase correlations B_χ and B_ϕ. Assuming line-of-sight propagation in a medium with sound speed and velocity fluctuations, a formulation can be derived based on the parabolic equation, the *first* Rytov approximation, assuming weak scattering, and the Markov approximation [1]. It can be noted that a derivation not using the Markov approximation has been presented [9], which leads to slightly different results. This is not considered in the model used here, but adjustments could be made in future work.

The resulting normalised mutual coherence function can be written as [1, Eq. 7.179]

$$\hat{\Gamma}(x, r) = \exp\left\{ -[B_\chi(x, 0) - B_\chi(x, r) + B_\phi(x, 0) - B_\phi(x, r)] \right\} \tag{5}$$

where $\mathbf{r_1}$ and $\mathbf{r_2}$ are replaced by a transverse separation distance r (see Fig. 1), assuming that the fluctuations are homogeneous and isotropic. In Eq. (5), the mutual coherence function has been normalised with the unperturbed amplitudes, i.e. divided by $|\hat{p}(x, 0)|^2$. The formulation of the normalised mutual coherence function in Eq. (5) is general in that it holds for both plane and spherical waves and for different turbulence models. Only the transverse correlation functions B_χ and B_ϕ need to be defined for the corresponding situation.

Eq. (5) may be rewritten in the form

$$\hat{\Gamma}(x, r) = \exp\left\{ -[B_\chi(x, 0) + B_\phi(x, 0)]\left[1 - \frac{B_\chi(x, r) + B_\phi(x, r)}{B_\chi(x, 0) + B_\phi(x, 0)}\right] \right\}. \tag{6}$$

Studying Eq. (6), relevant characteristics can be identified for sound propagation in a random medium. At zero transverse separation distance, i.e. for $r = 0$ in Eq. (6), the exponent is zero and the coherence is at maximum, i.e. the normalised mutual coherence function equals 1. When r increases, the correlations $B_\chi(x, r)$ and $B_\phi(x, r)$ will tend to zero, resulting in the mutual coherence function tending to a constant value given by

$$\hat{\Gamma}(x, r \to \infty) = \exp\left\{ -[B_\chi(x, 0) + B_\phi(x, 0)] \right\}. \tag{7}$$
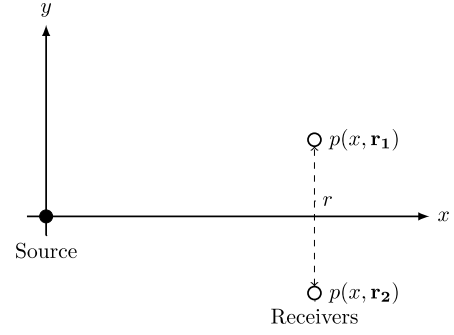

Fig. 1. Geometry for two receivers with transverse separation, r, and one source.

Since the correlation at $r = 0$ equals the variance of the fluctuation, i.e. $B_\chi(x, 0) = \langle \chi^2 \rangle$ and $B_\phi(x, 0) = \langle \phi^2 \rangle$, the above equation can also be rewritten as

$$\hat{\Gamma}(x, r \to \infty) = \exp\left\{ -[\langle \chi^2 \rangle + \langle \phi^2 \rangle] \right\}. \tag{8}$$

Using more compact notations, $g(x, r) = B_\chi(x, r) + B_\phi(x, r)$ and $\hat{g}(x, r) = g(x, r)/g(x, 0)$, Eq. (6) can be rewritten as

$$\hat{\Gamma}(x, r) = \exp\left\{ -g(x, 0)[1 - \hat{g}(x, r)] \right\}. \tag{9}$$

From Eq. (9) we can identify the essential connection between the sum of the transverse correlation functions, $g(x, r)$, and the resulting mutual coherence function, $\hat{\Gamma}(x, r)$. From a physics viewpoint, $g(x, 0)$ in Eq. (9) (which often is formulated as $2\gamma x$, where γ is the *extinction coefficient*) can be seen to cause an overall reduction of the coherent part of a sound wave propagating through a random medium. On the other hand, the factor $1 - \hat{g}(x, r)$ in Eq. (9) can be seen as a compensating factor, creating less reduction in coherence, since the paths to the two receiver positions involve wave propagation through partly the same randomnesses of the atmosphere.

It can here also be noted that in case the mutual coherence function is known, or assumed, but $B_\chi(x, r)$ and $B_\phi(x, r)$ are unknown, we can find the sum, $g(x, r) = B_\chi(x, r) + B_\phi(x, r)$, as

$$g(x, r) = \ln \frac{\hat{\Gamma}(x, r)}{\hat{\Gamma}(x, r \to \infty)}. \tag{10}$$

Here, Eq. (9) has been used together with noting that $\hat{\Gamma}(x, r \to \infty) = \exp[-g(x, 0)]$, i.e. $\ln[\hat{\Gamma}(x, r \to \infty)] = -g(x, 0)$. Assuming that $B_\chi(x, r) \approx B_\phi(x, r)$, we can thus find estimates of $B_\chi(x, r)$ and $B_\phi(x, r)$ based on the mutual coherence function by using Eq. (10).

Expressions for the transverse correlation functions $B_\chi(x, r)$ and $B_\phi(x, r)$ and for the mutual coherence function can be derived in closed form, as function of frequency, for quasi-homogenous and anisotropic random media, for plane and spherical waves and for different turbulence models [1]. The two turbulence models of main interest here are the von Karman model and the Gaussian model, where the former is physically based and the latter more convenient mathematically. The models can describe fluctuations in velocity and in temperature (or index of refraction), which are the two main variables of media randomnesses for atmospheric sound propagation [1].

The modelling examples studied here are simplified in that they assume transverse correlation functions and mutual coherence function for homogeneous and isotropic temperature fluctuations for plane waves, since the main purpose with this paper is to define and exemplify the essential parts of the modelling approach. These simplifications seem not to pose any restriction to future development of the approach to the more complex cases.

For homogeneous Gaussian temperature fluctuations in an isotropic atmosphere, the mutual coherence function for plane waves can be written as [1]

$$\hat{\Gamma}(x,r) = \exp\left[-\left(\langle\chi^2\rangle + \langle\phi^2\rangle\right)\left(1 - e^{-r^2/\ell^2}\right)\right] \tag{11}$$

where ℓ is the length scale of the temperature inhomogeneities and where

$$\langle\chi^2\rangle = \frac{\sqrt{\pi}k^2 x}{8}\left(1 + \frac{\arctan(D_T)}{D_T}\right)\frac{\sigma_T^2 \ell}{T_0^2} \tag{12}$$

$$\langle\phi^2\rangle = \frac{\sqrt{\pi}k^2 x}{8}\left(1 - \frac{\arctan(D_T)}{D_T}\right)\frac{\sigma_T^2 \ell}{T_0^2}. \tag{13}$$

Here, k is the acoustic wave number, i.e. $k = 2\pi f/c$, where f is the sound frequency and c the sound speed, $D_T = 4x/(k\ell^2)$ is a wave parameter, σ_T^2 is the variance of temperature fluctuations, and T_0 the mean temperature (in Kelvin). In Eqs. (12) and (13) the term $\arctan(D_T)/D_T$ can be neglected if $D_T \gg 1$ [1, Eq. 7.112], resulting in

$$\langle\chi^2\rangle = \langle\phi^2\rangle = \frac{\sqrt{\pi}k^2 x}{8} \cdot \frac{\sigma_T^2 \ell}{T_0^2}. \tag{14}$$

(It can be noted that $D_T \gg 1$ corresponds with applicability of Fraunhofer diffraction [1, Ch. 7]. It can also be noted that for D_T not larger than 1, the terms $\pm\arctan(D_T)/D_T$ cancel out when adding $\langle\chi^2\rangle$ and $\langle\phi^2\rangle$.)

Comparing Eq. (11) with Eq. (9), we can identify

$$\hat{g}(x,r) = \exp(-r^2/\ell^2) \tag{15}$$

for the Gaussian plane wave model.

For homogeneous and isotropic temperature fluctuations following instead the von Karman model, the mutual coherence function for plane waves can be written as [1]

$$\hat{\Gamma}(x,r) = \exp\left\{-\left(\langle\chi^2\rangle + \langle\phi^2\rangle\right)\left[1 - \frac{\Gamma_{1/6}}{\pi}\left(\frac{r}{2L_T}\right)^{5/6} K_{5/6}\left(\frac{r}{L_T}\right)\right]\right\} \tag{16}$$

where $\Gamma_{1/6}$ is the Gamma function evaluated at $1/6$, L_T is the von Karman length scale of temperature inhomogeneities, $K_{5/6}$ is a modified Bessel function of the second kind with order $5/6$ and

$$\langle\chi^2\rangle = \frac{\sqrt{\pi}\Gamma_{5/6}k^2 x}{4\Gamma_{1/3}}\left\{[1 + E(D_T)]\frac{\sigma_T^2 L_T}{T_0^2}\right\} \tag{17}$$

$$\langle\phi^2\rangle = \frac{\sqrt{\pi}\Gamma_{5/6}k^2 x}{4\Gamma_{1/3}}\left\{[1 - E(D_T)]\frac{\sigma_T^2 L_T}{T_0^2}\right\}. \tag{18}$$

Here, E is a function of the wave parameter for the von Karman case, $D_T = 4x/(kL_T^2)$, detailed in [1, Ch. 7], and for $D_T \gg 1$ it can be neglected, resulting in

$$\langle\chi^2\rangle = \langle\phi^2\rangle = \frac{\sqrt{\pi}\Gamma_{5/6}k^2 x}{4\Gamma_{1/3}} \cdot \frac{\sigma_T^2 L_T}{T_0^2}. \tag{19}$$

Comparing Eq. (16) with Eq. (9), we can identify, for the von Karman plane wave model, that

$$\hat{g}(x,r) = \frac{\Gamma_{1/6}}{\pi}\left(\frac{r}{2L_T}\right)^{5/6} K_{5/6}\left(\frac{r}{L_T}\right). \tag{20}$$

Corresponding formulas including velocity fluctuations, as well as for spherical wave propagation, are given by different right hand sides of Eqs. (11)–(13) and (16)–(18) [1, Ch. 7.3.1 & 7.3.2], with the property of interest here that the function $g(x,r)$ can be identified for each case, which is sufficient to uniquely define the mutual coherence function as shown above.

In the following it is assumed that the wave parameter, $D_T = 4x/(kL_T^2)$, for both the Gaussian and the von Karman models, is large,

such that the transverse correlation functions for log-amplitude and phase are equal, i.e.,

$$B_{\chi,\phi}(x,r) = \frac{g(x,r)}{2}. \tag{21}$$

Using Eq. (21), we have, for the Gaussian plane wave model for temperature fluctuations, using also Eqs. (14) and (15),

$$B_{\chi,\phi}^{\text{G}}(x,r) = \frac{\sqrt{\pi}k^2 x}{8} \cdot \frac{\sigma_T^2 \ell}{T_0^2}\exp(-r^2/\ell^2) \tag{22}$$

and for the von Karman plane wave model for temperature fluctuations, using also Eqs. (19) and (20),

$$B_{\chi,\phi}^{\text{vK}}(x,r) = \frac{\sqrt{\pi}\Gamma_{5/6}k^2 x}{4\Gamma_{1/3}} \cdot \frac{\sigma_T^2 L_T}{T_0^2} \cdot \frac{\Gamma_{1/6}}{\pi}\left(\frac{r}{2L_T}\right)^{5/6} K_{5/6}\left(\frac{r}{L_T}\right). \tag{23}$$

2.2. Method to produce sound signals

To produce sound signals fulfilling a specified mutual coherence function, realisations of log-amplitude and phase fluctuations are needed for the chosen transverse correlation function. Here, the random realisations of the log-amplitude and phase fluctuations ($\chi(r)$ and $\phi(r)$) are produced numerically via calculating the Fourier transform (FFT) of the correlation function with respect to transverse separation, r, giving an autospectrum in wave-number domain, and then calculating the inverse Fourier transform (IFFT) of the square root of the autospectrum multiplied by a phase factor (e.g. [3,10]). The resulting realisations of $\chi(r)$ and $\phi(r)$ follow independent normal distributions in amplitude and fulfil the prescribed correlation functions over space, r. Here, the correlation functions used as starting point are given by Eqs. (22) and (23). Their amplitudes are at first normalised such that $B_{\chi,\phi}(x,r) = \hat{g}(x,r)/2$, whereby the frequency dependence is removed, and later the realisations of $\chi(r)$ and $\phi(r)$ are scaled, as explained below.

The unperturbed sound signals are here given by realisations of Gaussian white noise as test signals. To add the effect of the random log-amplitude and phase fluctuations ($\chi(r)$ and $\phi(r)$), short-time blocks of the unperturbed sound signal are transformed to frequency domain and multiplied by $e^{\chi(r)+i\phi(r)}$, where r is updated for each block. (It can be noted that the block-wise modelling of the phase variation does not capture the frequency shift induced by a continuous phase variation.) The different frequency components of $\chi(r)$ and $\phi(r)$ are scaled with a factor proportional to frequency, according to Eqs. (22) and (23), and multiplied by a constant scaling factor to model the overall strength of the turbulence. The constant scaling factor also includes an amplitude correction factor of $e^{-\langle\chi^2\rangle}$ to compensate for the otherwise expected increase in power due to the log-amplitude fluctuations.[1] The scaling with frequency of $\chi(r)$ and $\phi(r)$ implies that different frequency components are assumed to be fully correlated, which may not be a valid approximation at high frequencies (e.g. [11]).

Furthermore, a limit is put on the size of the log-amplitude fluctuations due to the saturation effect (see e.g. [4]). Without considering the saturation, unrealistically large log-amplitude fluctuations may result at high sound frequencies for a fixed distance, x, and turbulence strength, σ_T. Here, the expected variance of the log-amplitude fluctuations has been limited to 0.6 (a value within the range of reported values, of about 0.5–0.8 [4]). Referring to Eqs. (14) and (19), the value of $\langle\chi^2\rangle$ is here allowed to increase with frequency until it reaches 0.6 and thereafter remain at that value.

To set the increase in r for successive blocks, and hence set the values of $\chi(r)$ and $\phi(r)$, an underlying velocity, U, is assumed for a source

---

[1] For a random variable, χ, being normally distributed with zero mean, it can be shown that the amplitude e^χ gives a root-mean-square change of $\langle e^{2\chi}\rangle^{1/2} = e^{\langle\chi^2\rangle}$.

moving in the transverse direction, such that $r = Ut$, where t is time, as further described in the following Section.

3. Results and discussion

3.1. Validation for direct sound

The above described approach to induce randomnesses in amplitude and phase is here evaluated by a comparison between the analytic mutual coherence functions as given by Eqs. (11) and (16) and their numeric estimates from using created time signals. For that purpose, $M = 100$ white noise signals (with zero mean and standard deviation equal to one) are generated with a length of 40 s at a sample rate of $f_s = 51.2$ kHz. To aid the numerical evaluation, the white noise signals are created by repeated identical blocks of $N_b = 4096$ samples. (The duration of each block is then 80 ms.) The underlying velocity is set to $U = 1.25$ m/s, which leads to a step size in the transverse separation of $\Delta r = U N_b / f_s = 0.1$ m for each block. (Although there is no Doppler effect considered in the current modelling, it could be included in future work.) In order to smooth the time signal, an overlap-add technique (OLA) is used where the blocks perturbed in log-amplitude and phase are overlapped by 50% with Hann window (see e.g. [12]). The supplementary material to this paper includes exemplifying sound clips.

Since the source position is changed from one block to the next, the transverse mutual coherence here manifests itself as a correlation between different blocks of the signal. Hence, the numerical evaluation of the mutual coherence function becomes similar to an estimate of the *autocorrelation* function of the produced signals. Denoting the signals $s_m(n)$, for realisation $m = 1 \dots M$, and where n is the discrete time step ($n = 0 \dots N - 1$, with time, $t = n/f_s$), a normalised, block-wise autocorrelation function of signal m can be written

$$\rho_{s_m, s_m}(i_b) = \frac{\sum_n s_m(n) s_m(n - i_b N_b)}{\sqrt{\sum_n s_m^2(n) \sum_n s_m^2(n - i_b N_b)}} \qquad (24)$$

where i_b is the block number. Since the generated signals are of finite length, the range of n will be limited when numerically applying the above equation. To estimate the expected value, a mean value of M realisations of $\rho_{s_m, s_m}(i_b)$ is calculated, leading to the numerical estimation of the mutual coherence function as

$$\hat{\Gamma}_{\text{num}}(i_b) = \frac{1}{M} \sum_m \rho_{s_m, s_m}(i_b). \qquad (25)$$

Since it is of interest to study the mutual coherence function at different frequencies of the sound signal, the perturbed signals are filtered into 1/3-octave bands from 25 Hz to 20 kHz before the estimate according to Eqs. (24)–(25) is made for each frequency band. Examples are calculated for the two turbulence models described above, i.e. Gaussian and von Karman temperature fluctuations for plane waves, at two strengths of turbulence. The strengths of the turbulence are chosen by setting the variance of the log-amplitude fluctuations and the phase fluctuations to either 0.04 or 0.4 at 1 kHz. Here, the length scales L_T and ℓ are both assumed to be 2 m. The numerical results are plotted together with the corresponding analytical solutions in Figs. 2–5 for the 1/3-octave bands 63, 250, 1000, 4000 and 16000 Hz. The analytical solutions have been subjected to the same limitations in log-amplitude fluctuations due to saturation as assumed for the numerical implementation. The overall agreement between numerical and analytical results is very good and, mainly at higher frequencies, minor deviations are shown when the transverse coordinate (i_b in Eq. (25)) departs from zero. Studying the general shapes of the mutual coherence functions, it can be seen that they decrease faster with increasing separation when the frequency is higher and when the overall variance scaling is higher, as expected. It can also be seen that the slope is less alternating for the von Karman turbulence model than for the Gaussian turbulence model, as expected since the latter gives a concentration of turbulence length
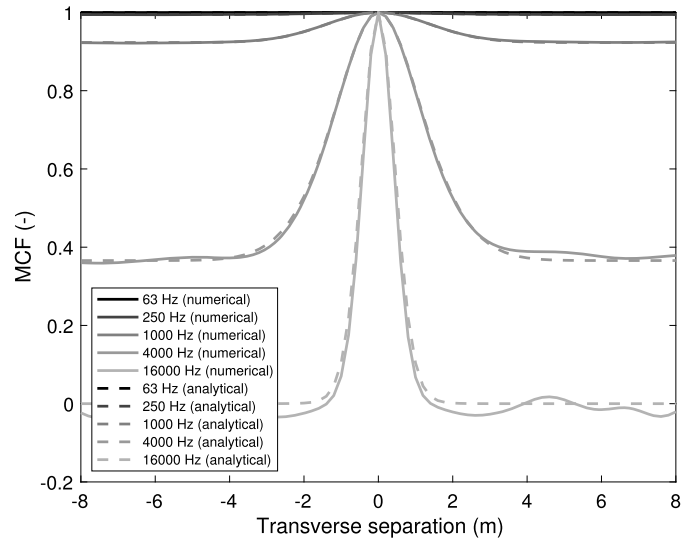

Fig. 2. Mutual coherence function (MCF) as function of transverse separation plotted for five 1/3-octave bands. Numerical and analytical results for Gaussian turbulence with variance 0.04 for the log-amplitude and phase fluctuations.
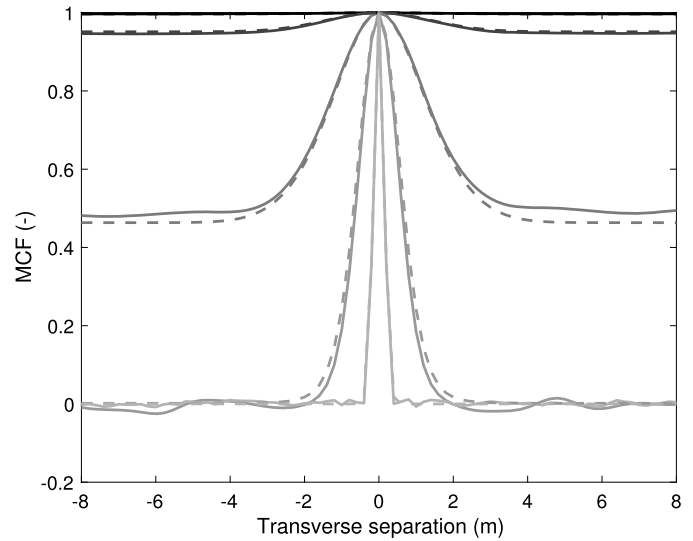

Fig. 3. Same as Fig. 2 except Gaussian turbulence with variance 0.4 for the log-amplitude and phase fluctuations.

scales close to a single value whereas the former better models real turbulence with a broader range of influencing length scales.

In Figs. 6–11 waterfall plots of the mutual coherence function over the entire frequency range for the von Karman turbulence model are shown for the numerical results, for the analytical results and for their difference. It can be seen that the overall agreement between numerical and analytical results is very good. The difference plots reveal significant deviations, less than 0.1, at higher frequencies whereas at low to mid frequencies, the deviations are very small.

3.2. Application of the method to a situation with a direct and a reflected propagation path

When a moving source is passing by a fixed receiver, the direct path from source to receiver changes over time. Assuming that the inhomogeneous properties of the medium that affect the sound propagation are fixed in space and do not change over time, the above described approach can be applied to model the pass-by of a source concerning the fluctuations in amplitude and phase of the direct path, i.e. the scintil-
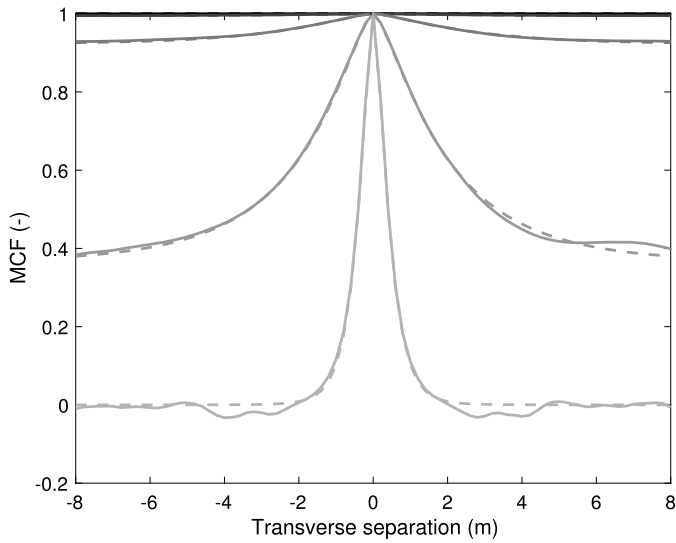
Fig. 4. Same as Fig. 2 except von Karman turbulence with variance 0.04 for the log-amplitude and phase fluctuations.
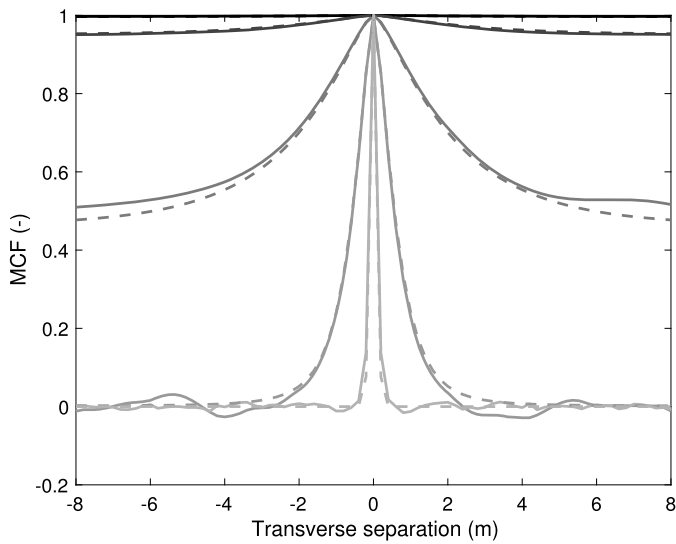

Fig. 6. Analytical mutual coherence function (MCF) as function of transverse separation and frequency. Results for von Karman turbulence with variance 0.04 for the log-amplitude and phase fluctuations.

Fig. 5. Same as Fig. 2 except von Karman turbulence with variance 0.4 for the log-amplitude and phase fluctuations.

Fig. 7. Numerical result for the same case as in Fig. 6.

lations due to the wave propagating along different paths through the medium, as well as the coherence between the direct sound and a contribution from a reflected path. It should be noted that the commonly used assumption of *frozen turbulence*, i.e. that the local properties of the medium can be treated as constant as the sound wave propagates through, also allows for a volume of frozen turbulence to move with the mean wind speed. Here, the turbulence is assumed be both frozen and non-moving; however, the modelling approach described here could be further developed for moving turbulence.

A receiver is placed between the straight line trajectory of the source and a flat reflecting object parallel to it, as depicted in Fig. 12. Assuming that the receiver is closer to the reflecting object than to the trajectory of the source, the dominating effect on the decorrelation, i.e. on the reduced coherence between the direct and the reflected path, will be determined by the range, D, and the transversal separation, r, as defined in Fig. 12. The effect of the random medium on the remaining part of the reflected path (dotted line in the figure) could be modelled by additions to its log-amplitude and phase fluctuations. This is omitted here but could be included in future work.
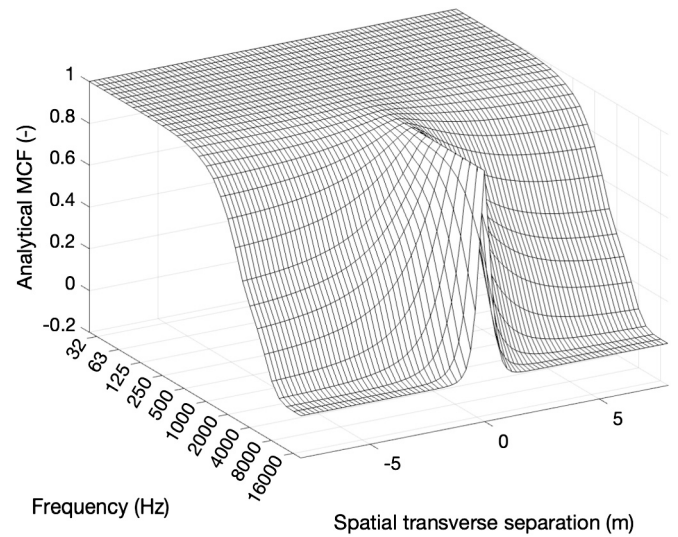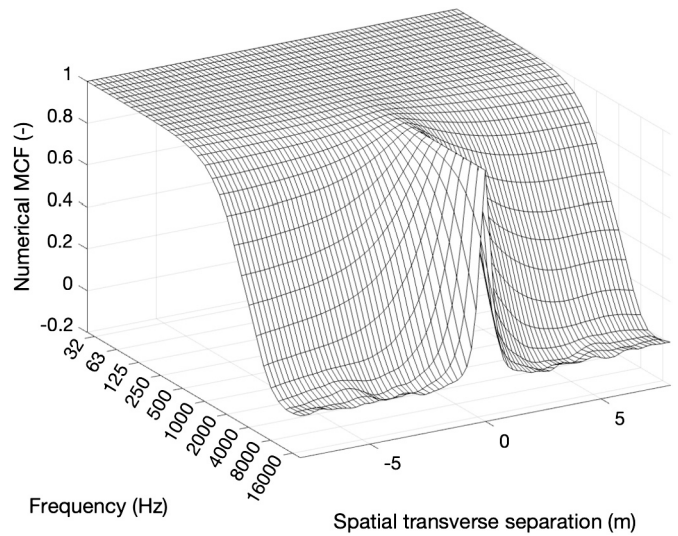
Using the notations in Fig. 12, the values of r and D can be found as follows. The separation distance is $r = 2D_0 \sin(\gamma/2)$, where $\gamma = \beta - \alpha = \tan^{-1}[(a_1 + 2a_2)/y] - \tan^{-1}(a_1/y)$ and $D_0 = \sqrt{y^2 + a_1^2}$. The range, D, is given by $D = D_0 \cos(\gamma/2)$. In the test calculations made here r is used for the mutual coherence function; however, the range, D, is assumed to be constant, with a value of a_1 (the direct distance at point of passage), to simplify the comparison between numerically produced results and theory. To set the fluctuations of both the direct and the reflected contribution, the transverse separation r, between the direct and the reflected path, is needed as well as the transverse separation r_0, i.e. between the direct path and a fixed reference (here at $y = 0$). In relation to the fixed reference ($y = 0$), the transverse distance to the direct path is r_0 and the transverse distance to the reflected path is $r_0 + r$, which are the actual inputs to determine the fluctuation in complex amplitude at each position y of the source. In the numerical calculations made here, the source moves forward along the y-axis in steps $\Delta y = U N_b/f_s = 0.1$ m and for each step the values of r_0 and $r_0 + r$ are updated.

At $y = 0$, r_0 has the same value as $r_0 + r$ ($r_0 = r = 0$) whereby the induced fluctuations to direct and reflected sound contributions are equal,
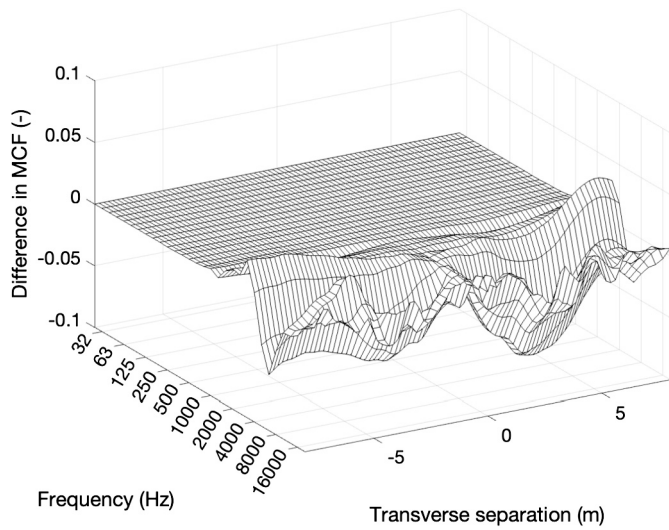
Fig. 8. Difference in mutual coherence function (MCF) between numerical and analytical results. (Results in Fig. 7 minus results in Fig. 6.)

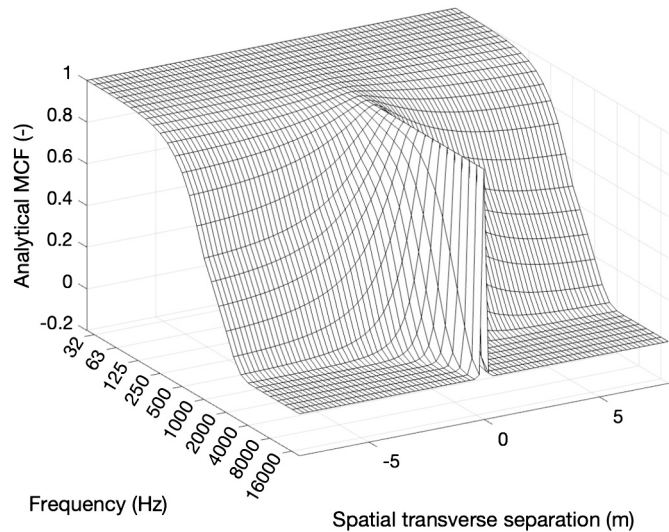**Fig. 10.** Numerical result for the same case as in Fig. 9.

Fig. 9. Analytical mutual coherence function (MCF) as function of transverse separation and frequency. Results for von Karman turbulence with variance 0.4 for the log-amplitude and phase fluctuations.

Fig. 11. Difference in mutual coherence function (MCF) between numerical and analytical results. (Results in Fig. 10 minus results in Fig. 9.)

whereas when y departs from 0, the induced fluctuations to direct and reflected contributions grow different. For the example modelled here, it is assumed that $a_1 = 60$ m and that the random medium is described according to the von Karman model with an outer length scale of $L_T = 1$ m. It could be noted that the values used here for the length scales are unusually small but could be motivated by an application to noise sources of surface transport like road or rail traffic, where sound propagation occurs close to the ground, for which the larger turbulence scales are not effective. The distance between the source line and the reflecting surface is assumed to be 80 m, i.e. $a_2 = 20$ m. Similarly to the previous numerical test, signals based on identical blocks of white noise are used, where the direct and the reflected sound signals are identical before the random fluctuations are induced. A set of M realisations of fluctuations in log-amplitude and phase are produced. For each realisation and for each step in y, both r_0 and $r_0 + r$ are updated and the corresponding fluctuations are applied to the amplitude and phase of the direct and reflected sound. The supplementary material to this paper includes several exemplifying sound clips, as further detailed below.

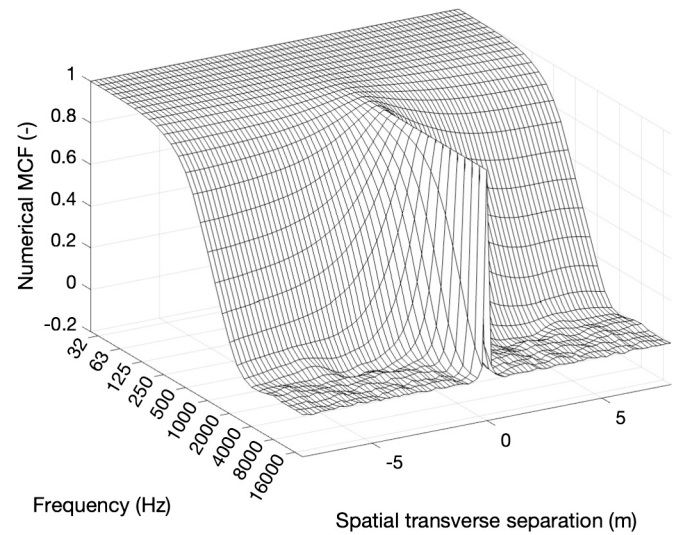From a set $m = 1 \ldots M$, $M = 100$, realisations, the normalised mutual coherence function between direct and reflected sound signals is estimated numerically. This corresponds to calculating the *correlation* between direct and reflected sound signals, which is different from the autocorrelation calculations made in the previous Section for validating the mutual coherence between different direct paths represented by different time-blocks.

Denoting the direct signal as $s_{m,d}$ and the reflected signal as $s_{m,r}$, first the correlation, C, for one realisation is calculated block-wise as

$$C_{s_{m,d},s_{m,r}}(i_b) = \frac{\sum_{n_b} s_{m,d}(n)s_{m,r}(n)}{\sqrt{\sum_{n_b} s_{m,d}^2(n) \sum_{n_b} s_{m,r}^2(n)}} \tag{26}$$

where n_b denotes all elements, n, within block i_b. To estimate the expected value, a mean value of M realisations of $C_{s_{m,d},s_{m,r}}(i_b)$ is calculated, leading to the numerical estimation of the mutual coherence function as

$$\hat{\Gamma}_{d,r,\text{num}}(i_b) = \frac{1}{M} \sum_m C_{s_{m,d},s_{m,r}}(i_b). \tag{27}$$

For evaluation with the analytical solution, the block i_b is translated to y-coordinate (each step in y equals $\Delta y = U N_b / f_s$) and thereafter to the transverse separation r, according to the geometrical description above. The numerical and analytical results are compared in Fig. 13, show-
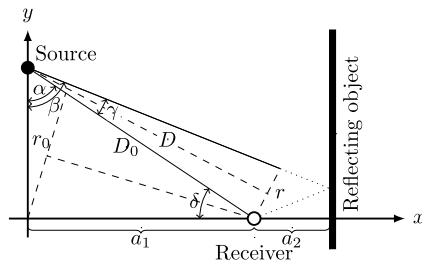
Fig. 12. Geometry for direct and reflected path from a source to a receiver.
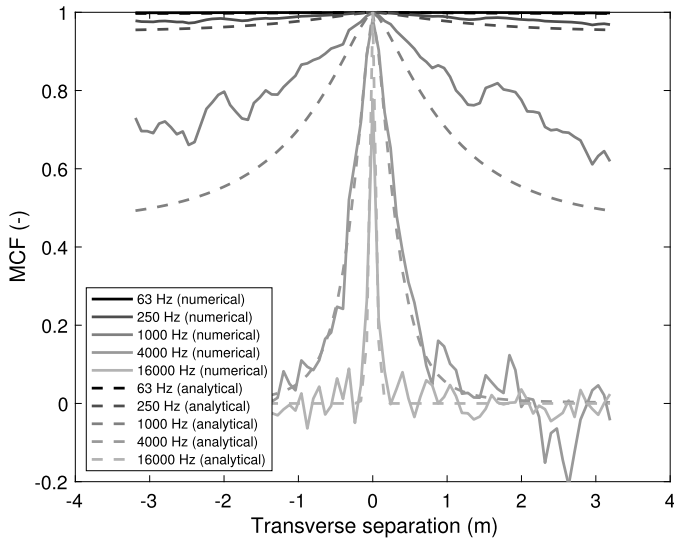

Fig. 13. Mutual coherence function (MCF) for the situation with direct and reflected sound. Plotted as function of transverse separation, *r*, for five 1/3-octave bands. Numerical and analytical results for von Karman turbulence with variance 0.4 for the log-amplitude and phase fluctuations.

ing reasonable agreement. It can be seen that the numerical results are less smooth compared with the analytical results. The noisier character compared with the results shown in Figs. 2–5 could be attributed to the averaging process, where the single-path analysis involves a summation over the whole length of the available signal whereas the analysis for the situation of direct and reflected sound contributions uses a summation over a single block. In Fig. 13 one can also see more systematic deviations between the numerical and the analytical results, most prominent at 1 kHz where the slope is large as function of frequency.

It can be noted that the fluctuations in amplitude and phase assumed here are unusually strong for the relatively short propagation distance of the calculated example. The standard deviation of the corresponding temperature fluctuations is about 3 degrees. However this is chosen for the purpose of the study to evaluate the suggested modelling approach. For future work, describing specific outdoor conditions, the modelling could include also velocity fluctuations, which in realistic cases may have a much larger influence on the fluctuations in amplitude and phase (e.g. [9]).

The supplementary material to this paper includes several example sound clips including direct sound, reflected sound and total sound. The direct sound is exemplified as both unperturbed signal and signal with fluctuations. For the total sound, the sound signals for the direct and the reflected paths are added. The distance of propagation, from source to receiver, for both the direct path and the reflected path, has been used to adjust the amplitude assuming spherical spreading. The first set of such sounds uses white noise in identical blocks, as described above. The second set uses continuous pink noise (without identical blocks) and the third set uses a more realistic truck engine sound. Each

sound clip is 6 s long and the point of passage is at 3 s, i.e. where the fluctuation is the same for direct and reflected sound. Listening to the total sound, a *phasing effect* is audible, i.e. spectral dips at frequencies that change over time. It is most prominent for the signals based on white noise, which have relatively more high-frequency content, but affect also the other signal types. It is expected that an inclusion of the Doppler effect, together with higher speeds of source movement, would have an influence on the phasing effect. However, this is not studied in the current paper.

4. Conclusions

The paper describes an approach to modelling the random fluctuations in amplitude and phase due to sound propagation in real outdoor environments, i.e. where atmospheric turbulence causes randomnesses in the propagation properties of the medium, and where the fluctuations are modelled on both single paths of propagation, in the form of scintillations and random time dalays, and on the coherence between a direct path and a reflected path from a source to a receiver. Realisations of scintillations for a single path, in form of amplitude and phase fluctuations, are produced and applied to sound signals, assuming a step-wise movement of the source through a frozen turbulence that follows a chosen turbulence model. Here, only temperature turbulence (or a corresponding random index of refraction) is considered, following either a Gaussian or a von Karman model for homogeneous and isotropic turbulence. Based on transverse correlation functions of the log-amplitude and phase fluctuations for plane waves, corresponding to the chosen turbulence model, realisations of fluctuations are produced where each realisation for a traversing source defines the fluctuations of the direct path, the fluctuations of the reflected path and the mutual coherence between the contributions from the two paths.

The method is described and validated using test signals for situations without reflection, showing very good agreement between the analytical mutual coherence function and its numerical estimate from multiple realisations, for the two turbulence models and for two turbulence strengths. The method, when applied to a situation with a reflecting surface, shows reasonable agreement. Sound clips exemplifying the method are provided as supplementary material to the paper.

5. Further work

The purpose of the paper was to describe a viable approach to including physics-based fluctuations when auralizing situations of environmental sounds. Such fluctuations in amplitude and phase need to fulfil a governing mutual coherence between different paths of propagation as resulting e.g. from a reflecting object or when the source has moved to a new position. These kinds of situations have been modelled here using simplifying assumptions with the purpose of validating the method. These assumptions may be relaxed and points of interest in further work include to model the Doppler effect, height-varying properties of the random medium, frozen turbulence moving with a mean speed, refraction due to wind and temperature gradient, additional effects of reflected paths including ground reflection as well as to include less simplified turbulence models. It is also of interest to investigate the effects from using the Rytov approximation in the auralization methodology and possible alternative approaches valid for strong scattering. Furthermore, the possibility of extending the modelling to include also reduced coherence of different frequency components is of interest.

CRediT authorship contribution statement

Jens Forssén: Writing – review & editing, Writing – original draft, Visualization, Validation, Methodology, Investigation, Formal analysis, Data curation, Conceptualization.

Declaration of competing interest

The authors declare the following financial interests/personal relationships which may be considered as potential competing interests: Jens FORSSEN reports financial support was provided by Chalmers University of Technology. Jens FORSSEN reports financial support was provided by Sweden's Innovation Agency. If there are other authors, they declare that they have no known competing financial interests or personal relationships that could have appeared to influence the work reported in this paper.

Data availability

No data was used for the research described in the article.

Appendix A. Supplementary material

Supplementary material related to this article can be found online at https://doi.org/10.1016/j.apacoust.2024.110038.

References

[1] Ostashev VE, Wilson DK. Acoustics in moving inhomogeneous media. second edition. CRC Press; 2015.

[2] Heutschi K, Pieren R, Müller M, Manyoky M, Wissen Hayek U, Eggenschwiler K. Auralization of wind turbine noise: propagation filtering and vegetation noise synthesis. Acta Acust Acust 2014;100(1):13–24. https://doi.org/10.3813/AAA.918682.

[3] Rietdijk F, Forssén J, Heutschi K. Generating sequences of acoustic scintillations. Acta Acust Acust 2017;103(2). https://doi.org/10.3813/AAA.919061.

[4] Bresciani APC, Maillard J, de Santana LD. Physics-based scintillations for outdoor sound auralization. J Acoust Soc Am 2023;154(2):1179–90. https://doi.org/10.1121/10.0020666.

[5] Arntzen M, Simons DG. Ground reflection with turbulence induced coherence loss in flyover auralization. Int J Aeroacoust 2014;13(5–6):449–62. https://doi.org/10.1260/1475-472X.13.5-6.449.

[6] Lincke D, Schumacher T, Pieren R. Synthesizing coherence loss by atmospheric turbulence in virtual microphone array signals. J Acoust Soc Am 2023;153(1):456–66. https://doi.org/10.1121/10.0016847.

[7] Habets EAP, Cohen I, Gannot S. Generating nonstationary multisensor signals under a spatial coherence constraint. J Acoust Soc Am 2008;124(5):2911–7. https://doi.org/10.1121/1.2987429.

[8] Pieren R, Lincke D. Auralization of aircraft flyovers with turbulence-induced coherence loss in ground effect. J Acoust Soc Am 2022;151(4):2453–60. https://doi.org/10.1121/10.0010121.

[9] Ostashev VE, Shabalina E, Wilson DK, Kamrath MJ. Non-Markov behavior of acoustic phase variance in the atmospheric boundary layer. In: Waves in random and complex; 2022.

[10] Forssén J. Calculation of noise barrier performance in a turbulent atmosphere by using substitute sources with random amplitudes. In: Proc. 9th long range acoustic propagation symposium; 2000. p. 16–26. https://research.chalmers.se/en/publication/23203.

[11] Ostashev VE, Kamrath MJ, Wilson DK, White MJ, Hart CR, Finn A. Vertical and slanted sound propagation in the near-ground atmosphere: coherence and distributions. J Acoust Soc Am 2021;150(4):3109–26. https://doi.org/10.1121/10.0006737.

[12] Rizzi SA, Sahai AK. Auralization of air vehicle noise for community noise assessment. CEAS Aeronaut J 2019;10(1):313–34. https://doi.org/10.1007/s13272-019-00373-6.